Elastic scattering of $^{10}C + ^{27}Al$

IOP Conf. Series: Journal of Physics: Conf. Series **876** (2017) 012001 doi:10.1088/1742-6596/876/1/012001

Elastic scattering of ^{10}C + ^{27}Al

E F Aguilera[1,*], J J Kolata[2], E Martinez-Quiroz[1], D Lizcano[1], P Amador-Valenzuela[1], A García-Flores[1,3], D W Bardayan[2], P D O'Malley[2], D S Monteiro[2,5], V. Morcelle[4], S. Carmichael[2], S L Henderson[2], D Blankstein[2], M R Hall[2], B Schultz[2], J Allen[2], J Kelly[2]

[1] Departamento de Aceleradores, Instituto Nacional de Investigaciones Nucleares, Apartado Postal 18-1027, C. P. 11801, México, D. F., México
[2] Physics Department, University of Notre Dame, Notre Dame, In, 46556-5670, USA
[3] Universidad Autónoma del Estado de México, Código Postal 50000, Toluca, México
[4] Departamento de Física, Universidade Federal Rural do Rio de Janeiro, 23851-970, Rio de Janeiro, Brasil
[5] Instituto Latino-Americano de Ciências da Vida e da Natureza - UNILA - Av. Tancredo Neves, 6731, Bl. 6. CEP 85867- 970 - Foz do Iguaçu, Paraná - Brasil

E-mail: *eli.aguilera@inin.gob.mx

Abstract. Preliminary results for the elastic scattering of the Super-Borromean nucleus ^{10}C on ^{27}Al are presented, at E_{lab} = 29 MeV. Taking the Sao Paulo potential as the bare potential, possible polarization potentials are investigated by adding a volume and a surface complex term to account for fusion and direct couplings, respectively. Besides an imaginary short-range potential to simulate the bulk of fusion, the best-fit polarization potential turns out to be real and has the effect of shifting the barrier radius up by 0.6 fm, thus suggesting a fusion enhancement.

1. Introduction

There has been considerable interest in studying Borromean nuclei, which can be described as nuclei having a three-cluster structure with the additional property that the removal of any of the three clusters leads to an unbound two-body system. The name "Borromean" is borrowed from the so called Borromean rings in mathematics, which consist of three topological circles which are linked in such a way that removing any ring results in two unlinked rings. Their use in the coat of arms of the aristocratic Borromeo family in Northern Italy (15^{th} century) suggested the name.

There is also one known case of a four-cluster nucleus with Borromean properties, the ^{10}C nucleus, which can be described as two alpha particles plus two protons. In this case, the removal of any one of the four clusters produces an unbound three-cluster system, which has led some authors to call this a Super-Borromean nucleus [1]. More precisely, this is an example of a 4^{th} order Brunnian link [2].

With the aim of investigating the behaviour of this exotic nucleus in interactions with light heavy-ions, an elastic scattering angular distribution has been measured for the ^{10}C + ^{27}Al system for an energy E_{lab} = 29 MeV. Preliminary results of these measurements are shown in the present work, as well as the results of corresponding optical model analyses.

The experimental procedure is described in Sec. 2) as well as the preliminary results and a comparison with previous data for a similar system. An appropriate optical model analysis is described in Sec. 3 and, finally, a summary and the main conclusions of this work will be presented in Section 4.

2. Experimental procedure and results

A primary 42 MeV ^{10}B beam was obtained from the FN Tandem accelerator at the University of Notre Dame (UND). This beam impinged on a ^{3}He primary target which was contained into a gas cell held at 1 atm pressure. The secondary ^{10}C beam was thus obtained through the n-p exchange reaction ^{3}He(^{10}B, ^{10}C). In addition to ^{10}C, satellite beams of ^{10}B and ^{11}C were also produced, with smaller yields of lighter beams such as Be and Li isotopes. In order to separate between reactions induced by the different secondary projectiles, the beam was bunched and the respective time-of-flight was measured. After bunching, the typical yields were 40 particle-nA for the primary beam and 3.9×10^{4} ^{10}C/sec for the secondary beam.

Three E-ΔE telescopes made of Silicon surface barrier (SSB) detectors were used at the most forward angles, while three additional single SSB detectors were used at larger angles. The most forward telescope had a 7 mm collimator while the diameter of the remaining detectors varied between 10 and 22 mm. Figure 1 shows the experimental setup. The collimator-target distance was 15 cm for the left-hand detectors and 18 cm for the right-hand ones. The target was an Al foil with thickness 158.7 μg/cm^2. A 2.59 mg/cm^2 Au target was also used for normalization purposes.

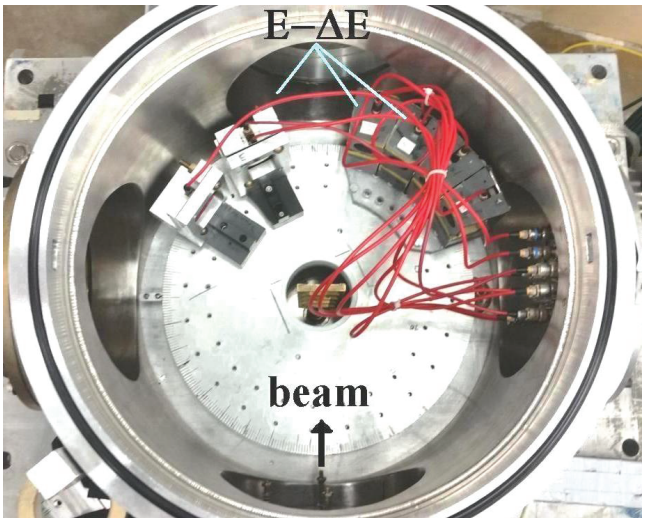

Figure 1. Experimental setup. As indicated, three SSB E-ΔE telescopes were used while the remaining three were single SSB detectors.

The plate holding the detectors (Fig. 1) was rotated twice so that three different angular configurations were measured, covering the angular range $15^\circ \leq \theta_{lab} \leq 65^\circ$. Figures 2 and 3 show examples of the typical ΔE vs E and T vs E spectra illustrating the achieved separation of the elastic ^{10}C groups.

Figure 4 presents the obtained angular distribution for ^{10}C on ^{27}Al (circles). For comparison, data previously reported [3] for the neighboring (normal) system ^{12}C + ^{27}Al (squares) are also shown, which correspond to a similar energy in the center of mass reference frame ($E_{c.m.} \sim 21$ MeV).

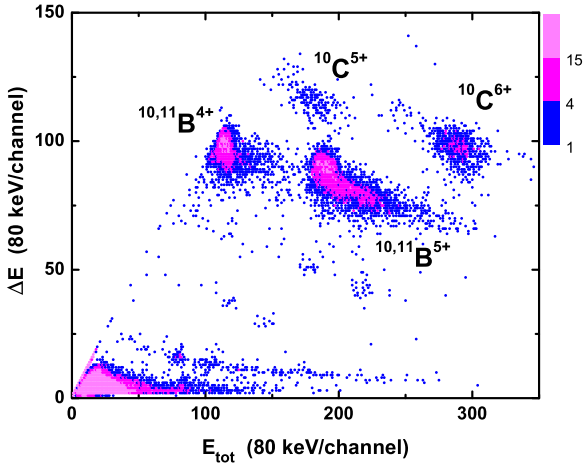

Figure 2. Typical ΔE vs E spectrum, taken at $E_{lab} = 29.5$ MeV and $\theta_{lab} = 30°$.

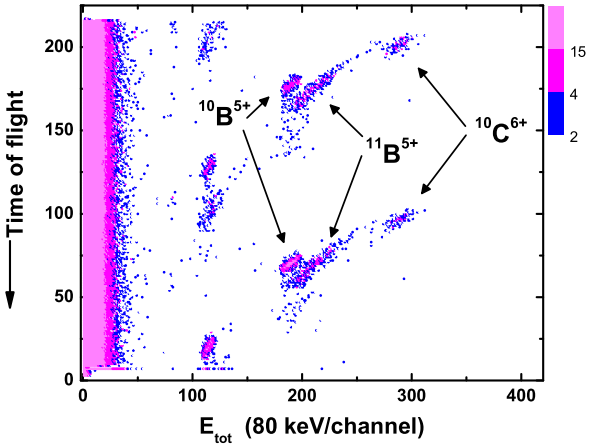

Figure 3. Typical Time-Of-Flight vs Energy spectrum, taken at $E_{lab} = 29.5$ MeV and $\theta_{lab} = 30°$.

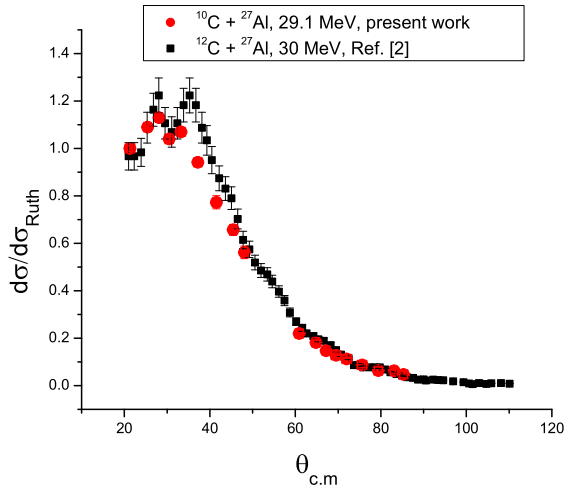

Figure 4. Experimental angular distribution obtained for the ^{10}C on ^{27}Al system at $E_{lab} = 29$ MeV. Both statistical uncertainties and estimated angle uncertainties have been included. For comparison, earlier data [3] reported for the stable ^{12}C on ^{27}Al system at nearly the same energy in the center of mass reference frame are also shown.

The structure shown by the ^{12}C data around 30° is also insinuated in the ^{10}C results, but much less pronounced. In addition, relative to the ^{12}C data, the angular distribution for the exotic system seems to be damped for angles in the region $35° \leq \theta_{c.m.} \leq 45°$. At the most backward angles, both angular distributions coincide. Because of the mass difference between ^{10,12}C, it should be more appropriate to transform the angle into distance of closest approch (see Sect. 3.2) to make the comparison. This is done in Fig. 5.

Qualitatively, the above observations remain valid if one replaces 30° by 2.5 fm and " 35° $\leq \theta_{c.m.} \leq$ 45° " by " 1.9 fm $\leq d \leq$ 2.3 fm " in the above paragraph. In next section, an optical model analysis will be performed for ^{10}C + ^{27}Al.

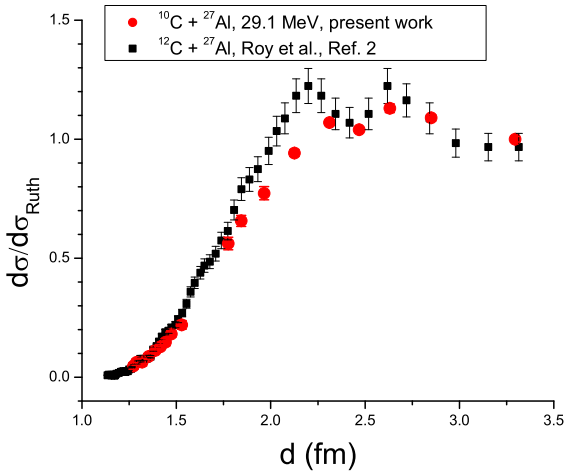

Figure 5. Same as Fig. 4, but $\theta_{c.m.}$ has been mapped into the distance of closest approach (see Sect. 3.2).

3. Optical model analysis

It's been long known that the parameter-free São Paulo Potential (SPP) [4] can be used as an appropriate bare potential to describe fusion reactions. Crema *et al.* [5], for example, have shown that the SPP gives reliable results in the analysis of fusion reactions with stable weakly-bound projectiles. Among other results, this fact has been used to show that the experimental fusion excitation functions for neutron-halo projectiles are suppressed with respect to the corresponding SPP predictions for energies above the respective Coulomb barriers, while those for proton-halo systems are enhanced [7, 8].

Additional evidence exists that at least for another proton-rich nucleus, ^{7}Be, a fusion enhancement above the barrier can be observed [8,9], albeit weaker than that in the proton-halo case. Since ^{10}C is also a proton-rich nucleus, it would be interesting to investigate whether a fusion enhancement might be expected from its interaction with other nuclei. Fusion data have not been measured for the present system, but an optical model analysis of the elastic scattering data might shed some light on this issue.

Within the framework of the optical model, fusion has been described as the absorption in a short-range imaginary potential interior to the barrier, W_{int}. Such a potential effectively simulates an incoming-wave boundary condition, thus giving a good barrier penetration model (BPM) prediction. In order for the fusion cross section calculated this way to be realistic, the optical model wave function should correctly describe the respective elastic scattering angular distribution. So, an appropriate polarization potential should be usually added to the bare potential. Assumedly, this polarization potential would result from respective couplings to fusion and direct channels. It has been shown for many systems that it is reasonable to decompose the total polarization potential into a direct and a fusion part [10–18]. With this in mind, the following general form for the total optical potential is proposed:

$$U_{TOT} = SPP + V_{Coul} + W_{int} + U_F + U_S, \quad (1)$$

where SPP is the bare (Sao Paulo) potential, V_{Coul} is the Coulomb potential, W_{int} is a short range Woods-Saxon potential (interior to the barrier: $W_0 = 50$ MeV, $r_0 = 1.$ fm, $a_0 = 0.2$ fm),

and U_F, U_S are complex polarization potentials that can be associated to couplings to the fusion and direct channels, respectively. U_F (U_S) is taken as having a volume (derivative) Woods-Saxon shape, where in each case the radius and difussenes are the same for both, the respective real and imaginary parts. To be more specific, $U_{F,S}$ can be written as

$$U_{F,S} = V_{F,S} + iW_{F,S}, \tag{2}$$

where V_F (V_S) and W_F (W_S) have identical radius and diffuseness.

3.1. Case of no polarization potential

The code FRESCO and its search version, SFRESCO [19], were used to perform all optical model calculations. As a reference, a calculation using SPP for the real part and 0.78×SPP for the imaginary part was performed. This combination has been shown to provide a good description of many systems [4]. For the present case, the result is illustrated with the dashed line in Fig. 6, which evidently does not follow the data. This indicates that the present system falls out of the systematics and should be dealt with separately.

The case where both U_F and U_S are zero was also calculated and it is shown with the dotted line in Fig. 6 (label SPP + W$_{int}$). Clearly, a non-zero polarization potential is necessary to describe the data.

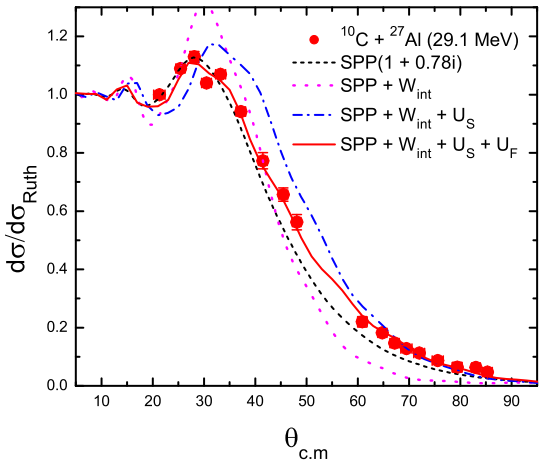

Figure 6. Optical model calculations, as explained in the text.

3.2. Purely direct polarization potential

In a first trial, the fusion part U_F in eq. 1 is assumed to be zero. As a guide to choose values for the geometric parameters r$_S$, a$_S$ (reduced radius and diffuseness, respectively) of the Woods-Saxon potential whose derivative will give U_S, a transformation $\theta_{c.m.} \rightarrow d$ is performed on the data. In this transformation, d is the reduced distance of closest approach on a Rutherford trajectory, given by

$$D = d(A_p^{1/3} + A_t^{1/3}) = \frac{1}{2} D_0 \left(1 + \frac{1}{sin(\theta_{c.m.}/2)}\right), \quad with\ D_0 = \frac{Z_p Z_t e^2}{E_{c.m.}}. \tag{3}$$

The transformed data are shown in Fig. 7, where the solid curve represents a fit of the data with the function

$$f(x) = \frac{a}{1 + exp[-k(x - x_c)]}, \tag{4}$$

where a, k and x_c are free parameters whose best-fit values are given in the inset of the figure. The strong absorption distance, d_S, corresponds to the point where the ratio $d\sigma/d\sigma_{Ruth} = 0.25$ and is calculated from $f(x)$ as $d_S = 1.55$ fm.

If one assumes that the falling down of the data with decreasing d is due only to the surface potential U_S, it is reasonable to take the radius of this potential as $r_S = d_S = 1.55$ fm, with an appropriate diffuseness to reproduce the slope of $f(d)$ (solid curve), such as does the dotted curve in Fig. 7. This gives $a_S = 0.9$ fm. The strength given in the inset ($W_{S0} = 0.666$) has no physical meaning and was chosen (along with a_S) to match the right wing of the dotted curve to the solid curve. The actual strengths of U_S (V_{S0}, W_{S0}) will be obtained from fitting the experimental angular distribution.

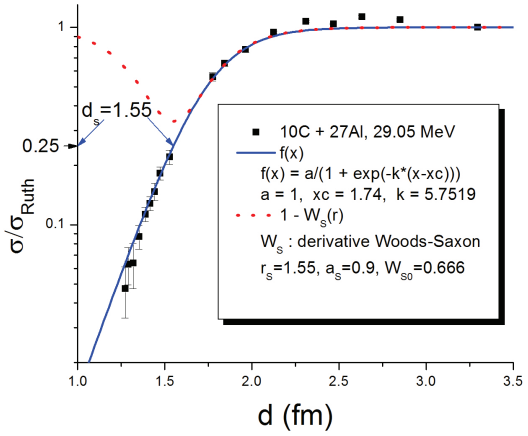

Figure 7. Plot of $d\sigma/d\sigma_{Ruth}$ vs d for the $^{10}C + ^{27}Al$ system. The meaning of the curves is explained in the inset and in the text.

The best fit is obtained for V_{S0} = -0.7 MeV, $W_{S0} = 0$, but a good description of the data is not achieved (χ^2/N = 38), as shown by the dash-dotted line in Fig. 6 (label SPP + W_{int} +U_S). This probably means that the falling down of the data with decreasing d should be produced by a combination of a fusion and a direct polarization potential.

3.3. Fusion and direct polarization potentials

The fusion polarization potential U_F will now be included, with radius and diffuseness values of $r_F = 1.4$ fm, $a_F = 0.43$ fm. These values have been used in similar descriptions of other systems, for instance the ^{6}Li + ^{208}Pb system [12]. Keeping these values fixed, the four strengths V_{F0}, W_{F0}, V_{S0}, W_{S0} were varied. The radius and diffuseness of the direct part, r_S, a_S were also varied, but with the constraint that their sum should be fixed at the value derived in the previous section, *i.e.*, $r_S + a_S = 1.55 + 0.9 = 2.45$ fm. This constraint would in principle guarantee the intuitive expectation that the shape of the surface potential should be able to partially match the solid curve in Fig. 7. This procedure yielded the best-fit values $V_{F0} = 14.87$ MeV, $W_{F0} = 0$, V_{S0} = -0.53 MeV, $W_{S0} = 0$, $r_S = 1.77$ fm, $a_S = 0.68$ fm. Varying the value of r_F around 1.4 fm did not improve the fit, which yielded χ^2/N = 2.8 as a final value. The respective results are represented by the solid curve in Fig. 6 (label SPP +W_{int} +U_S + U_F).

Notice that null absorptive potentials are obtained for both the fusion and the direct parts, with real polarization potentials which are attractive (repulsive) for the fusion (direct) part. This is illustrated in Fig. 8. Comparing the bare (solid curve) with the total (dashed curve) potential, one concludes that the polarization potentials have the effect of shifting the barrier

radius up by 0.63 fm, while the barrier height remains nearly unchanged. Since the fusion cross section varies roughly as the square of the barrier radius, a fusion enhancement is predicted by these results. The fact that W_{int} is the only imaginary part in the final potentials appearing in eq. 1, does actually imply that the fusion cross section would saturate the total reaction cross section at the present energy, which according to the present calculations amounts to σ_R (or σ_{Fus}) = 976 mb. Further experimental data are needed to corroborate the validity of these conclusions.

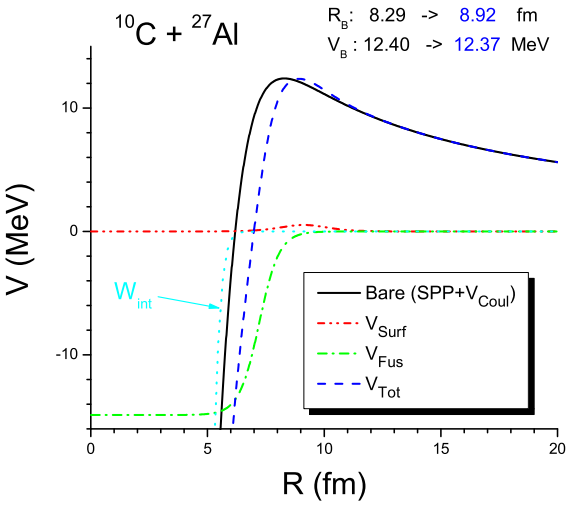

Figure 8. Different potentials involved in the OMP calculations. The final results for the direct, the fusion, and the total real potentials are represented by dash-double dot, dash-dot, and dashed curves, respectively. The bare (SPP) plus Coulomb potential is shown with the solid line, while the imaginary interior potential W_{int} is displayed with dots.

4. Conclusions

Preliminary data for the elastic scattering angular distribution of the ^{10}C + ^{27}Al system are presented, corresponding to $E_{c.m.}$ = 21.2 MeV (1.7×V_B). Comparison with reported data for the system ^{12}C + ^{27}Al at the same energy in the center of mass reference frame, indicates substantial differences. A purely surface (direct) polarization potential can not describe the data but introducing in addition a volume (fusion) potential, a good description is achieved. The best-fit polarization potential is non-absorptive, with the fusion (direct) part providing an attractive (repulsive) term. Altogether, the net effect is to shift the barrier radius up by 0.6 fm, thus predicting a fusion enhancement above the barrier. It would be interesting to corroborate this prediction with corresponding fusion measurements.

Acknowledgments

This work has been partially supported by CONACYT (México) and by NSF (USA) under grant No. PHY14-01343.

References

[1] Curtis N, Achouri N, Ashwood N, Bohlen H, Catford W, Clarke N, Freer M, Haigh P, Laurent B and Orr N 2008 *J. Phys.: Conf. Series* **111** 012022
[2] Brunn H 1892 Über Verkettung, S.-B.Math.-Phys.KI. Bayer Akad. Wiss. **22** 77
[3] Roy A, Frawley A D and Kemper K W 1979 *Phys. Rev.* C **20** 2143
[4] Chamon L C, Carlson B V, Gasques L R, Pereira D, De Conti C, Alvarez M A G, Hussein M S, Cândido Ribeiro M A, Rossi Jr. E S and Silva C P 2002 *Phys. Rev.* C **66** 014610
[5] Crema E, Chamon L C and Gomes P R S 2005 *Phys. Rev.* C **72** 034610
[6] Crema E, Gomes P R S and Chamon L C 2007 *Phys. Rev.* C **75** 037601
[7] Aguilera E F 2016 *J. Phys.: Conf. Series* **730** 012002

[8] Kolata J J ,Guimarães V and Aguilera E F 2016 *Eur. Phys. J.* A **52** 123
[9] Martinez-Quiroz E, Aguilera E F, Lizcano D, Amador-Valenzuela P, García-Martínez H, Kolata J J, Roberts A, Lamm L O, Rogachev G, Guimarães V, Becchetti F D, Villano A, Ojaruega M, Febbraro M, Chen Y, Jiang H, DeYoung P A and Peaslee G F 2014 *Phys. Rev.* C **90** 014616
[10] Kim B T, Naito M and Udagawa T 1990 *Phys. Lett.* B **237** 19
[11] Kim B T, So W Y, Hong S W and Udagawa T 2002 *Phys. Rev.* C **65** 044616
[12] So W Y, Udagawa T, Kim K S, Hong S W and Kim B T 2007 *Phys. Rev.* C **75** 024610
[13] Gómez-Camacho A and Aguilera E F 2004 *Rev. Mex. Fis.* **50** Supl. 3, 265
[14] Gómez-Camacho A and Aguilera E F 2004 *Nucl. Phys.* A **735** 425
[15] Gómez-Camacho A, Aguilera E F, Gomes P R S , Lubian J and Padron I 2007 *Nucl. Phys.* A **787** 275c
[16] Gómez-Camacho A, Gomes P R S, Lubian J, Aguilera E F and Padron I 2007 *Phys. Rev.* C **76** 044609
[17] Gómez-Camacho A, Aguilera E F, Lubian J and Gomes P R S 2013 *J. Phys. G: Nucl. Part. Phys.* **40** 035103
[18] Gómez-Camacho A and Aguilera E F 2014 *Phys. Rev.* C **90** 064607
[19] Thompson I 1988 *Comp. Phys. Rep.* **7** 167